Mechanistic study of chenodeoxycholic acid targeting pyruvate kinase to regulate hepatic lipid metabolism

XIAO ZHANG, SONGLIN TAN and XINHUA ZHOU

Department of Gastroenterology, Pingxiang People's Hospital, Pingxiang, Jiangxi 337000, P.R. China

Received July 6, 2025; Accepted December 8, 2025

DOI: 10.3892/br.2026.2179

Abstract. Non-alcoholic fatty liver disease (NAFLD) is the most prevalent chronic liver disease globally. Chenodeoxycholic acid (CDCA), a key component of bile acids, improves hepatic lipid metabolism. The present study aimed to investigate whether CDCA regulates hepatic lipid metabolism by interacting with pyruvate kinase (PK), and to elucidate the underlying molecular mechanism. High-fat cell and murine models were generated. The levels of total cholesterol (TC), triglycerides (TG), superoxide dismutase (SOD) and malondialdehyde (MDA) in cells and animal livers were measured. BODIPY and Oil Red staining were employed to detect the lipid droplet content. Reverse transcription-quantitative PCR was used to assess the expression of the lipid-related genes. Immunoprecipitation and molecular docking were used to examine the interaction between CDCA and PK, as well as their interaction sites. The effects of their binding on PK activity and pyruvate synthesis were investigated. Both *in vitro* and *in vivo* experiments demonstrated that compared with the high-fat group, the TG, TC and MDA levels in the CDCA-treated group were markedly reduced. In addition, lipid droplet count was markedly decreased and SOD activity was increased. The mRNA expression levels of lipid synthesis genes (such as fatty acid synthase and sterol regulatory element-binding transcription factor 1) were notably decreased, whereas those of lipid metabolism genes (CTP synthase 1 and peroxisome proliferator-activated receptor α) exhibited the opposite trend. CDCA specifically bound to the PK-M2 subtype, which promoted PK activity and pyruvate production. Pretreatment with a PK inhibitor completely reversed lipid synthesis inhibition and β-oxidation enhancement induced by CDCA. CDCA notably ameliorated hepatic lipid deposition, and its underlying mechanism was revealed to be closely associated with the direct binding of CDCA to PK and subsequent enhancement of PK activity.

Introduction

With the transformation of lifestyles and the increase in the obesity rate, non-alcoholic fatty liver disease (NAFLD) has become the most common chronic liver disease worldwide (1). According to a systematic review and meta-analysis, ~25% of adults are affected by NAFLD globally, and its incidence is still on the rise (1). The core pathological feature of NAFLD is excessive lipid deposition in the liver, which not only impairs liver function but is also closely related to disorders of glucose and lipid metabolism (2). A number of clinical studies have shown that patients with NAFLD often have metabolic abnormalities, such as insulin resistance, hyperglycemia, and hyperlipidemia (3,4). These metabolic disorders are intertwined, further increasing the risk of serious complications such as cardiovascular diseases and type 2 diabetes, posing a notable threat to patient health and quality of life.

Bile acids are important products of liver metabolism and serve key roles in lipid metabolism. Chenodeoxycholic acid (CDCA), a notable component of bile acids, has received considerable attention in previous years (5). Previous research has demonstrated that CDCA can improve hepatic lipid metabolism, as evidenced by animal experiments where triglyceride and cholesterol contents in animal livers were markedly reduced and beneficial changes occurred in the expression of lipid metabolism-related genes after CDCA intervention (6). However, its specific molecular mechanism has not been fully elucidated, limiting its further application in the treatment of fatty liver.

Pyruvate kinase (PK), a key rate-limiting enzyme in the glycolysis pathway, catalyzes the conversion of phosphoenolpyruvate to pyruvate and simultaneously generates ATP, providing energy for cells (7). In previous years, an increasing number of studies have shown that PK serves an important role in the regulation of hepatic lipid metabolism (8-10). Changes in the activity and expression levels of PK can affect fatty acid synthesis and oxidation, thereby affecting the balance of hepatic lipid metabolism (7). However, there are currently relatively few studies on whether there is an interaction between

Correspondence to: Dr Xiao Zhang, Department of Gastroenterology, Pingxiang People's Hospital, 8 Wugongshan Middle Avenue, Anyuan, Pingxiang, Jiangxi 337000, P.R. China
E-mail: zgym394qt@outlook.com

Abbreviations: NAFLD, nonalcoholic fatty liver disease; CDCA, chenodeoxycholic acid; TC, cholesterol; TG, triglyceride; SOD, superoxide dismutase; MDA, malondialdehyde; PK, pyruvate kinase

Key words: non-alcoholic fatty liver disease, chenodeoxycholic acid, pyruvate kinase, glycolysis

CDCA and PK and how this interaction affects hepatic lipid metabolism.

The present study aimed to explore whether CDCA regulates hepatic lipid metabolism by interacting with PK. This not only helps to reveal the potential molecular mechanism of CDCA in improving hepatic lipid metabolism, and enriches the understanding of the mechanism of bile acids in hepatic lipid metabolism, but also provides novel targets and a theoretical basis for the treatment of fatty liver, with important theoretical significance and clinical application value.

Materials and methods

Cell culture. The human normal hepatocyte cell line THLE-2 was purchased from American Type Culture Collection (ATCC; cat. no. CRL-2706), and human hepatoma cells HepG2 were purchased from ATCC (cat. no. HB-8065) and preserved in the laboratory. All cell lines used in the present study were authenticated using short tandem repeat (STR) profiling (Genewiz, Inc.) within 6 months prior to experimentation, and the STR profiles of THLE-2 and HepG2 matched the reference databases (ATCC), confirming no cross-contamination. The THLE-2 cells were cultured in BEGM™ Bronchial Epithelial Cell Growth Medium (cat. no. CC-3170; Lonza Group, Ltd.), which included 5 ng/ml EGF, 0.5 μg/ml hydrocortisone, 0.5 μg/ml epinephrine, 10 μg/ml transferrin, 5 μg/ml insulin, 0.1 ng/ml retinoic acid, 6.5 ng/ml triiodothyronine and 50 μg/ml gentamicin/amphotericin B. HepG2 cells were cultured in DMEM (cat. no. SH30243.01; HyClone™; Cytiva) containing 10% fetal bovine serum (FBS; Gibco; cat. no. 10099-141; Thermo Fisher Scientific, Inc.) and 1% penicillin-streptomycin (cat. no. P1400; Beijing Solarbio Science & Technology Co., Ltd.), and both cell lines were routinely cultured in an incubator at 37˚C and 5% CO_2.

High-fat (HF) cell model. When the confluence of THLE-2 and HepG2 cells reached 70-80%, the medium was replaced with serum-free DMEM containing oleic acid (OA; cat. no. P1145; Sigma-Adrich; Merck KGaA) and palmitic acid (PA; cat. no. P5585; Sigma-Adrich; Merck KGaA). Various OA/PA combinations were tested (0.25/0.125, 0.5/0.25 and 1.0/0.5 mM) and the cells were induced for 24 h. The concentrations (0.5 mM OA + 0.25 mM PA) were selected because this combination induced optimal lipid droplet accumulation (as detected by BODIPY staining) without excessive cytotoxicity [viability >80% via Cell Counting Kit-8 (CCK-8) assay (Beyotime Institute of Biotechnology); data not shown]. For the CCK-8 assay, 10 μl of CCK-8 solution was added to the cells after 48 h of culture. The cells were then incubated for an additional 2 h, and the absorbance at 450 nm (OD value) was measured using a microplate reader. Cells were divided into the following groups for treatment: The control group, normal cultured THLE-2 and HepG2 cells; the HF group, cells induced with OA/PA without additional treatment; the CDCA group, during HF induction, 10 and 50 μM CDCA (cat. no. HY-76847; MedChemExpress) were added for intervention; and the CDCA + Shikonin (cat. no. HY-N0822; MedChemExpress) group, 1 h before adding 50 μM CDCA for intervention, 10 μM Shikonin was added for pretreatment. Each group had 6 replicate wells and subsequent detection was performed after 24 h of treatment.

BODIPY staining. THLE-2 and HepG2 cells were fixed in 4% ice-cold paraformaldehyde (cat. no. P0099; Beyotime Institute of Biotechnology) at 4˚C for 20 min, then treated with 0.1% Triton X-100 (Beyotime Institute of Biotechnology) at room temperature for 5 min, and washed twice with phosphate-buffered saline (PBS) to remove the residual 4% paraformaldehyde. A working fluid solution containing 10 μM BODIPY 493/503 (cat. no. GC42959; GLPBIO Technology LLC) was added to the cells, and the mixture was incubated at 37˚C for 30 min in the dark. Subsequently, the cell nuclei were stained with DAPI at room temperature for 5 min after two washes with PBS. After three more washes with PBS, the cells were immediately imaged using a fluorescence microscope (IX73; Olympus Corporation) at a magnification of x200. The area and fluorescence intensity of the lipid droplets were quantified using ImageJ software (version 1.8.0; National Institutes of Health) by analyzing five random fields per well (6).

Animal model. All animal experiments were performed in compliance with all relevant ethical regulations for animal testing and research and in accordance with the animal protocols approved (approval no. SW-2020R0126-F03) by Pingxiang People's Hospital (Pingxiang, China). A total of 24 male, 6-week-old C57BL/6J mice were purchased from Beijing Vital River Laboratory Animal Technology Co., Ltd. The mice were housed in SPF-grade animal rooms with controlled temperature (22±2˚C), humidity (50±10%), and a 12-h light/dark cycle. Each cage contained 6 mice (to ensure social interaction). Sterile food and filtered water were provided *ad libitum*. After 1 week of adaptive feeding in an SPF-grade animal room, the experiment was performed. The NAFLD model was established by feeding the mice a high-fat diet (HFD; cat. no. D12492; 60% fat content Research Diets, Inc.) for 12 weeks. Successful NAFLD modeling was determined based on body weight, with mice in the HF group exhibiting a body weight ≥20% higher than the normal diet group (average HF group weight ~38 g vs. normal group ~31 g).

After successful NAFLD modeling, 18 mice were randomly divided into three groups (n=6): i) A high-fat diet group (HF); ii) HF + CDCA (50 mg/kg/d); and iii) HF + CDCA (100 mg/kg/d). A normal diet group (fed with normal feed) was used as a control (n=6). During the entire study period, all the mice included at the start were monitored closely. There were no exclusions or losses; all mice completed the experimental procedures as scheduled, which ensured the integrity and reliability of the experimental data. The normal feed (cat. no. D12450B; Research Diets, Inc.) contained 10% fat, 70% carbohydrate and 20% protein, which was used as a direct contrast to the HFD (60% fat). CDCA (purity ≥98%; MedChemExpress) was dissolved in 0.5% carboxymethylcellulose sodium solution (cat. no. HY-Y0703; MedChemExpress) and administered by oral gavage at the corresponding dose once a day for 8 weeks. The total experiment duration (21 weeks) included 1 week of adaptation, 12 weeks of HFD feeding, and 8 weeks of CDCA intervention.

Table I. Primer sequences for reverse transcription-quantitative PCR.

Genes	Forward primer (5'→3')	Reverse primer (5'→3')	Organisms
FASN	CACAGTGCTCAAAGGACATGCC	CACCAGGTGTAGTGCCTTCCTC	Mus musculus
	TTCTACGGCTCCACGCTCTTCC	GAAGAGTCTTCGTCAGCCAGGA	Homo sapiens
SREBP-1c	CCGTAGAGAAGCTTGGCGAT	CACTAGAGGTCGGCATGGTC	Mus musculus
	ACTTCTGGAGGCATCGCAAGCA	AGGTTCCAGAGGAGGCTACAAG	Homo sapiens
CPT1α	GACCGCGCTCTTAGGACTAC	GAGCAGCAAGGAAGGACACT	Mus musculus
	GATCCTGGACAATACCTCGGAG	CTCCACAGCATCAAGAGACTGC	Homo sapiens
PPARα	AGAGGGCTGAGCGTAGGTAA	ATTGGGCCGGTTAAGACCAG	Mus musculus
	TCGGCGAGGATAGTTCTGGAAG	GACCACAGGATAAGTCACCGAG	Homo sapiens
GAPDH	CATCACTGCCACCCAGAAGACTG	ATGCCAGTGAGCTTCCCGTTCAG	Mus musculus
	GTCTCCTCTGACTTCAACAGCG	ACCACCCTGTTGCTGTAGCCAA	Homo sapiens

FASN, fatty acid synthase; SREBP-1c, sterol regulatory element-binding transcription factor 1; CTP1α, CTP synthase 1; PPARα, peroxisome proliferator-activated receptor α.

After the intervention, the mice were weighed and fasted for 12 h without water deprivation. For blood collection, 50-60 mg/kg sodium pentobarbital was administered intraperitoneally (anesthetic route, intraperitoneal injection) to induce temporary anesthesia, and 0.2 ml of blood was collected by eyeball enucleation. The animals were euthanized using an intraperitoneal overdose of sodium pentobarbital (100 mg/kg body weight; euthanasia method, intraperitoneal injection of anesthetic overdose). Death was verified by: i) No spontaneous breathing (chest movement) or heartbeat (chest palpation) for ≥5 min; and ii) no hind paw withdrawal reflex when pinched with forceps.

During the experiment, mice were monitored daily for health (coat condition, wounds, jaundice) and behavior (activity, feeding/drinking); body weight was measured weekly. Humane endpoints for euthanasia included: Severe weight loss (>20% of initial weight in 1 week), persistent lethargy/refusal to eat/drink for >24 h, visible organ damage (abdominal distension, and jaundice), or abnormal behaviors (trembling, convulsions). No mice met these endpoints or died unexpectedly; all 24 mice were euthanized at the end of the intervention.

The serum was separated, and the liver was quickly removed and fixed in 4% paraformaldehyde at 4˚C for 24 h. After fixation, the tissues were dehydrated and then cut into 8-10 μm-thick frozen sections using a cryostat. The sections were air-dried at room temperature for 10 min, followed by staining with freshly prepared Oil Red O (Thermo Fisher Scientific, Inc.) working solution at room temperature for 20 min in the dark. Finally, the stained sections were mounted with glycerol gelatin, and lipid droplet morphology was observed under a bright-field light microscope (Nikon E100) at a magnification of x400 (scale bar, 10 μm) and the remaining tissue was frozen at -80˚C for biochemical and molecular biology detection.

Determination of total cholesterol (TC), triglyceride (TG), malondialdehyde (MDA) and superoxide dismutase (SOD) contents. After cell collection, the cell lysate [2% Triton X-100 (Beyotime Institute of Biotechnology) lysate] was added to the cell pellet and incubated for 30 min to completely lyse the cells. Experiments were performed according to the instructions of the following kits: TC and TG detection kits (cat. nos. A111-1-1 and A110-1-1; Nanjing Jiancheng Bioengineering Institute), and SOD (cat. no. BC0170) and MDA (cat. no. BC0020) detection kits (Beijing Solarbio Science & Technology Co., Ltd.).

Reverse transcription-quantitative PCR (RT-qPCR). Total RNA from HepG2 cells or mouse liver tissues was extracted using TRIzol® reagent (cat. no. 15596026; Inivtrogen; Thermo Fisher Scientific, Inc.), reverse-transcribed into cDNA (cat. no. RR037A; Takara Bio, Inc.), and qPCR reactions of lipid synthesis [fatty acid synthase (FASN) and sterol regulatory element-binding transcription factor 1 (SREBP-1c)] and β-oxidation [CTP synthase 1 (CPT1α) and peroxisome proliferator-activated receptor α (PPARα)]-related genes were performed with SYBR Green Master Mix (cat. no. 04707516001; Roche Diagnostics), according to the manufacturer's instructions. The thermocycling conditions were as follows: An initial denaturation step was performed at 95˚C for 10 min. This was followed by 40-45 cycles consisting of three sequential steps of denaturation at 95˚C for 10 sec, annealing at 60˚C for 20 sec, and elongation at 72˚C for 20 sec. After the cycling stage, a final extension step was conducted at 72˚C for 3 min. GAPDH was used as an internal reference gene, and the relative gene expression was calculated using the $2^{-\Delta\Delta C}$ method (11). The primer sequences for the target and reference genes are listed in Table I.

Detection of PK activity and pyruvate. Experiments were performed according to the instructions of the PK activity detection kit and pyruvate detection kit (cat. nos. BC0540 and BC2200; Beijing Solarbio Science & Technology Co., Ltd.).

Co-immunoprecipitation (co-IP) and high-performance liquid chromatography (HPLC) detection. To determine the binding site of CDCA and PK, after treating cells with CDCA, the cells were lysed in Pierce™ RIPA Buffer (cat. no. 89900; Thermo Fisher Scientific, Inc.) to extract the total

protein, and a PK antibody was added for IP. For each IP reaction, 500 μl of normalized cell lysate (containing 1,000 μg total protein) was incubated with 2 μg of anti-PK polyclonal antibody (cat. no. ab137852; Abcam), while normal rabbit IgG (cat. no. ab37415; Abcam) at the same amount was used as the negative control. Prior to use, 20 μl of settled Protein A agarose beads (cat. no. 20334; Thermo Fisher Scientific, Inc.) were pre-washed three times with cold PBS to remove the storage buffer, and then added to the antibody-lysate mixture for binding. After eluting the bound protein, the CDCA content was determined using HPLC. A Waters-C18 chromatographic column (250x4.6 mm; 5 μm) was used, with a volume flow rate of 1 ml/min, an injection volume of 20 μl, a column temperature of 30˚C and a mobile phase consisting of 0.1% formic acid aqueous solution (A phase) and acetonitrile (B phase) at a ratio of 40:60. Under these chromatographic conditions, the retention time of CDCA was 8.5±0.2 min, which was used to confirm the specificity of CDCA detection.

Molecular docking to simulate the spatial structure interaction. Discovery Studio software (version 2023; BIOVIA; Dassault Systèmes) was used to dock the small-molecule structure of CDCA with the crystal structure of PK, and to analyze the key amino acid residues and binding modes of their interaction.

Statistical analysis. Experimental data are expressed as the mean ± standard deviation (SD) with the number of independent replicates indicated in the figure legends or corresponding table notes. The experimental data were analyzed using one-way analysis of variance using SPSS Statistics software (Version 21.0; IBM Corp.), followed by Tukey's honestly significant difference (HSD) test for post hoc multiple comparisons. P<0.05 was considered to indicate a statistically significant difference. Origin 2024b software (OriginLab Corporation) was used to create the graphs.

Results

CDCA ameliorates hepatic lipid deposition. The effect of CDCA on hepatic lipid deposition was evaluated with both *in vitro* and *in vivo* experiments. Screening of OA/PA combinations (0.25/0.125, 0.5/0.25 and 1.0/0.5 mM) revealed that 0.5 mM OA combined with 0.25 mM PA induced optimal lipid droplet accumulation without significant cytotoxicity (cell viability >80% as determined using a Cell Counting Kit-8 assay; data not shown). Following the establishment of the cell model using 0.5 mM OA combined with 0.25 mM PA, 10 and 50 μM CDCA were applied for 24-h intervention. The results demonstrated that compared with the HF group, intracellular TG content was significantly reduced in the CDCA-treated groups (P<0.05), with a comparable trend observed in HepG2 cells (Fig. 1A). TC content also exhibited a significant reduction (Fig. 1A), indicating that CDCA effectively mitigated intracellular lipid accumulation.

BODIPY staining visually illustrated intracellular lipid deposition. Abundant lipid droplets were observed in the HF group cells, whereas both the number and volume of lipid droplets were markedly decreased in the CDCA-treated groups, further confirming the inhibitory effect of CDCA on cellular lipid deposition (Fig. 1B). Additionally, cellular oxidative stress indices were assessed. Results indicated that, compared with the HF group, intracellular MDA content was significantly decreased in the CDCA-treated groups (P<0.05), while SOD activity was significantly elevated (Fig. 1C). To further investigate the molecular mechanisms underlying CDCA-mediated regulation of hepatic lipid metabolism, RT-qPCR analysis was performed. Results revealed that, in cell-based experiments, mRNA expression levels of lipid synthesis-related genes (FASN and SREBP-1c) were significantly downregulated following CDCA treatment compared with the HF group, whereas expression of lipid metabolism-related genes (CTP1α and PPARα) exhibited an opposite trend (Fig. 1D).

In the *in vivo* experiments, for the NAFLD mouse model established by 12-week HFD feeding, 50 and 100 mg/kg/d of CDCA were administered via gavage for 8-week intervention. The biochemical detection results showed that, compared with the HF group, the TC in the high-dose CDCA-treated group and TG in the high- and low-dose CDCA-treated groups were significantly reduced (P<0.01; Fig. 2A). Oxidative stress analysis in the liver showed that, compared with the HF group, the MDA content in the liver tissues of the CDCA-treated groups was significantly reduced (P<0.05), and the SOD activity was significantly increased (Fig. 2B). Oil Red O staining of liver tissue sections showed that the livers of mice in the HF group were filled with numerous red lipid droplets, whereas the lipid droplets in the CDCA-treated groups were notably reduced, especially in the high-dose group. Hepatic lipid deposition was markedly improved, which was consistent with the biochemical results, indicating that CDCA also reduced hepatic lipid deposition *in vivo* (Fig. 2C). In the liver tissues of mice, the mRNA expression levels in the high-dose CDCA-treated group of lipid synthesis genes, such as FASN and SREBP-1c, were significantly decreased compared with those in the HF group, and the expression of fatty acid β-oxidation-related genes (CPT1α and PPARα) were significantly upregulated (Fig. 2D), indicating that CDCA improved hepatic lipid deposition by inhibiting fatty acid synthesis and promoting fatty acid β-oxidation.

CDCA directly binds to PK and regulates its activity. To explore whether there was a direct interaction between CDCA and PK, a co-IP experiment was performed. After treating HepG2 cells with CDCA, the cells were lysed to extract the total protein, and a PK antibody was added for co-IP. The results showed that in the CDCA-treated group, CDCA bound to PK was successfully detected, while no obvious binding signal was detected in the control group, indicating specific binding between CDCA and PK (Fig. 3A). Furthermore, the results of molecular docking showed that CDCA specifically binds to the PK-M2 subtype. The binding site was mainly located in the catalytic domain of PK-M2, and the key amino acid sites were Arg246, Lys247, Glu275, Arg278 and Arg279 in PKM2. The binding free energy score between CDCA and PK-M2 was -10.33 kcal/mol, indicating a strong binding stability between the two molecules (Fig. 3B). To study the regulatory effect of CDCA on PK activity, intracellular PK activity was measured. The results showed that CDCA enhanced PK activity in a concentration-dependent

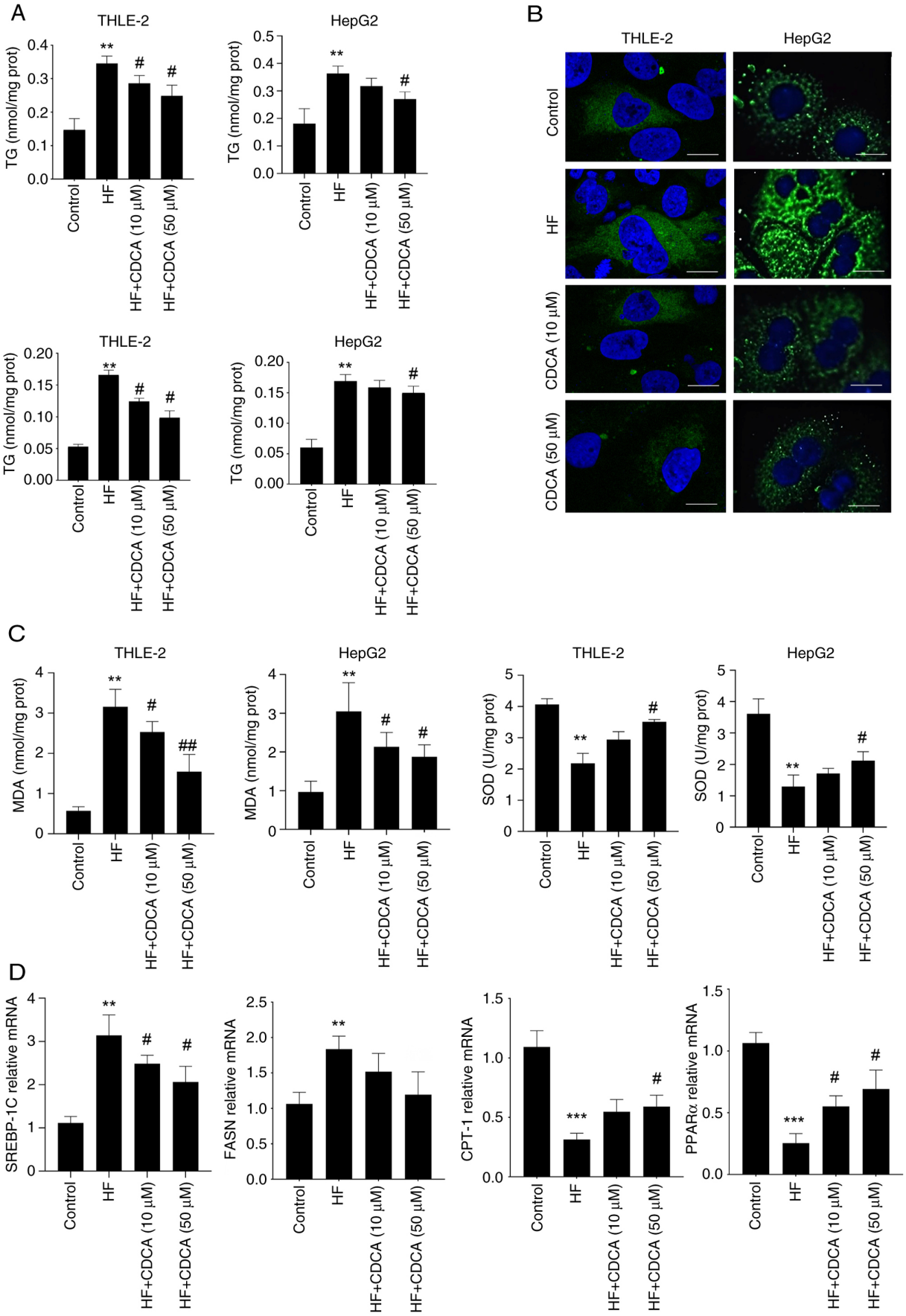

Figure 1. CDCA alleviates lipid deposition at the cellular level (n=4). (A) Intracellular TG and TC contents. (B) BODIPY staining of intracellular lipid droplets (magnification, x400; scale bar, 10 μm). (C) Intracellular MDA contents and SOD activities. (D) Reverse transcription-quantitative PCR detection of FASN, SREBP-1c, CTP-1 and PPARα. **P<0.01 and ***P<0.001 vs. control; $^{\#}$P<0.05 and $^{\#\#}$P<0.01 vs. HF. Error bars represent the standard deviation. CDCA, chenodeoxycholic acid; TG, triglycerides; TC, total cholesterol; MDA, malondialdehyde; SOD, superoxide dismutase; FASN, fatty acid synthase; SREBP-1c, sterol regulatory element-binding transcription factor 1; CTP1α, CTP synthase 1; PPARα, peroxisome proliferator-activated receptor α; HF, high fat.

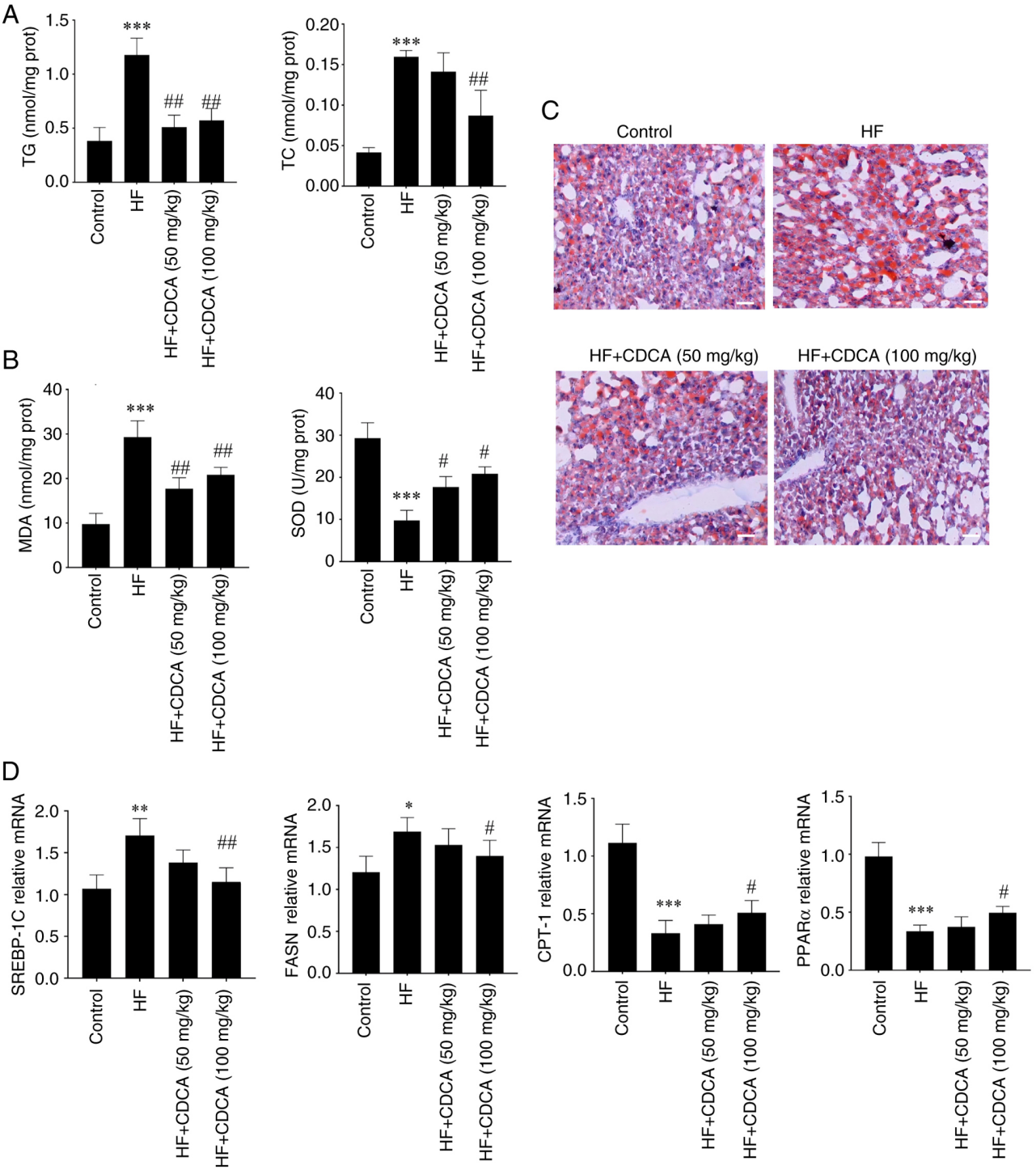

Figure 2. CDCA alleviates lipid deposition *in vivo* (n=6). (A) TG content and TC contents in the liver. (B) MDA content and SOD activity in liver tissues. Reverse transcription-quantitative PCR detection of FASN, SREBP-1c, CTP-1 and PPARα. (C) Oil Red O staining of lipid droplets in liver tissues (magnification, x200; scale bar, 20 μm). (D) Reverse transcription-quantitative PCR detection of FASN, SREBP-1c, CTP-1 and PPARα. *P<0.05, **P<0.01 and ***P<0.001 vs. control; $^{\#}$P<0.05 and $^{\#\#}$P<0.01 vs. HF. Error bars represent the standard deviation. CDCA, chenodeoxycholic acid; TG, triglycerides; TC, total cholesterol; MDA, malondialdehyde; SOD, superoxide dismutase; SREBP-1c, sterol regulatory element-binding transcription factor 1; CTP1α, CTP synthase 1; PPARα, peroxisome proliferator-activated receptor α; HF, high fat.

manner. When the CDCA concentration was in the range of 10-50 μM, the PK activity gradually increased with increasing CDCA concentration, and the difference was statistically significant (P<0.05; Fig. 3C). The enhancement of PK activity promoted the production of pyruvate, a product of glycolysis process (Fig. 3D), indicating that CDCA affects glycolysis by regulating PK activity.

PK mediates the regulation of hepatic lipid metabolism by CDCA. To verify the role of PK in the CDCA-mediated improvement of hepatic lipid metabolism, a functional rescue experiment was performed. HepG2 cells were pretreated with 10 μM of the PK inhibitor (Shikonin) 1 h before intervention with 50 μM CDCA. These results showed that Shikonin pretreatment completely reversed

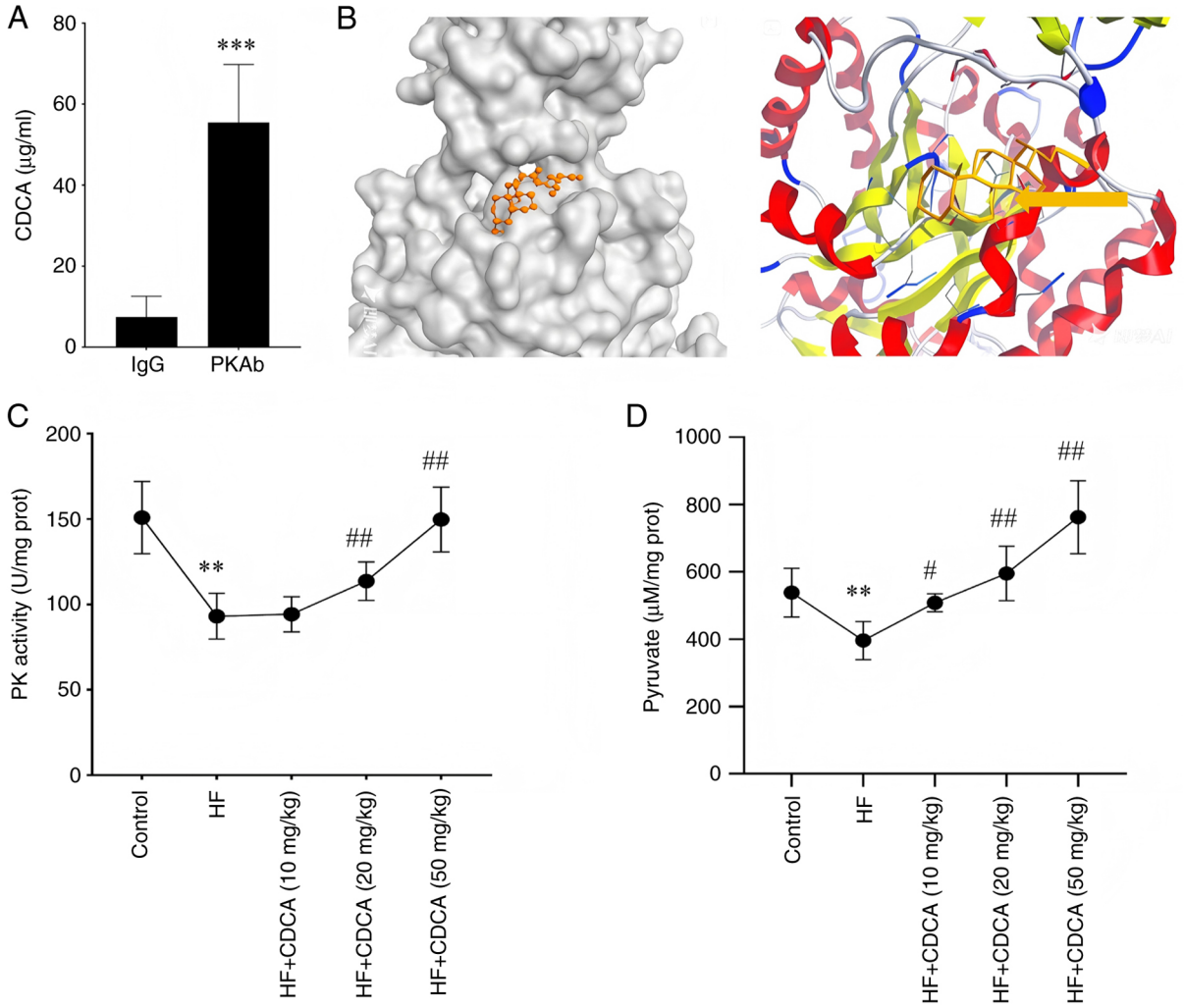

Figure 3. CDCA directly binds to PK and regulates its activity (n=4). (A) Detection of CDCA by co-immunoprecipitation combined with high-performance liquid chromatography. ***P<0.001 vs. IgG. (B) Molecular docking results show that CDCA specifically binds to the PK-M2 subtype. (C) Intracellular PK activity. (D) Intracellular pyruvate concentration. **P<0.01 vs. control; #P<0.05 and ##P<0.01 vs. HF. Error bars represent the standard deviation. CDCA, chenodeoxycholic acid; PK, pyruvate kinase; HF, high-fat.

the inhibitory effect of CDCA on lipid synthesis and enhanced β-oxidation. Compared with the CDCA-alone treatment group, the intracellular TG and TC levels in the CDCA + Shikonin group were significantly increased (P<0.01; Fig. 4A).

Immunofluorescence results showed that the fluorescence intensity of carbohydrate-responsive element-binding protein (ChREBP) in the nucleus was markedly reduced in the CDCA-treated group, whereas the nuclear translocation of ChREBP was restored in the CDCA + Shikonin group, and the fluorescence intensity in the nucleus was enhanced (Fig. 4B). Meanwhile, the CDCA-PK interaction promoted the nuclear localization of PPARα (Fig. 4B). Concurrently, 50 μM CDCA treatment reduced the mRNA expression levels of FASN and SREBP-1c, and these reduced levels returned to a state similar to the baseline after Shikonin intervention. By contrast, the mRNA expression levels of CPT1α and PPARα were increased following 50 μM CDCA treatment, and this upregulatory effect was reversed by Shikonin (Fig. 4C), indicating that PK serves a key mediating role in the regulation of hepatic lipid metabolism by CDCA.

Discussion

To the best of our knowledge, for the first time, the present study revealed a direct interaction between CDCA and PK and demonstrated that this interaction promotes PK activation and pyruvate production. A previous study has shown that CDCA mainly improves hepatic lipid metabolism by activating the farnesoid X receptor (FXR) (12). After FXR activation, on the one hand, CDCA was demonstrated to inhibit the expression of cholesterol 7α-hydroxylase, reducing the synthesis of bile acids. By contrast, it was also shown to promote the expression of fibroblast growth factor 15 (FGF15). FGF15, in turn inhibited hepatic fatty acid synthesis and cholesterol uptake through a negative feedback mechanism, thereby reducing hepatic lipid content (13). However, the present study found that the interaction between CDCA and PK provides a novel pathway for improving hepatic lipid metabolism.

CDCA specifically binds to the PK-M2 subtype and notably enhances PK activity by stabilizing enzyme conformation. As a key rate-limiting enzyme in glycolysis, enhanced activity of PK accelerates glycolysis, resulting in a marked increase

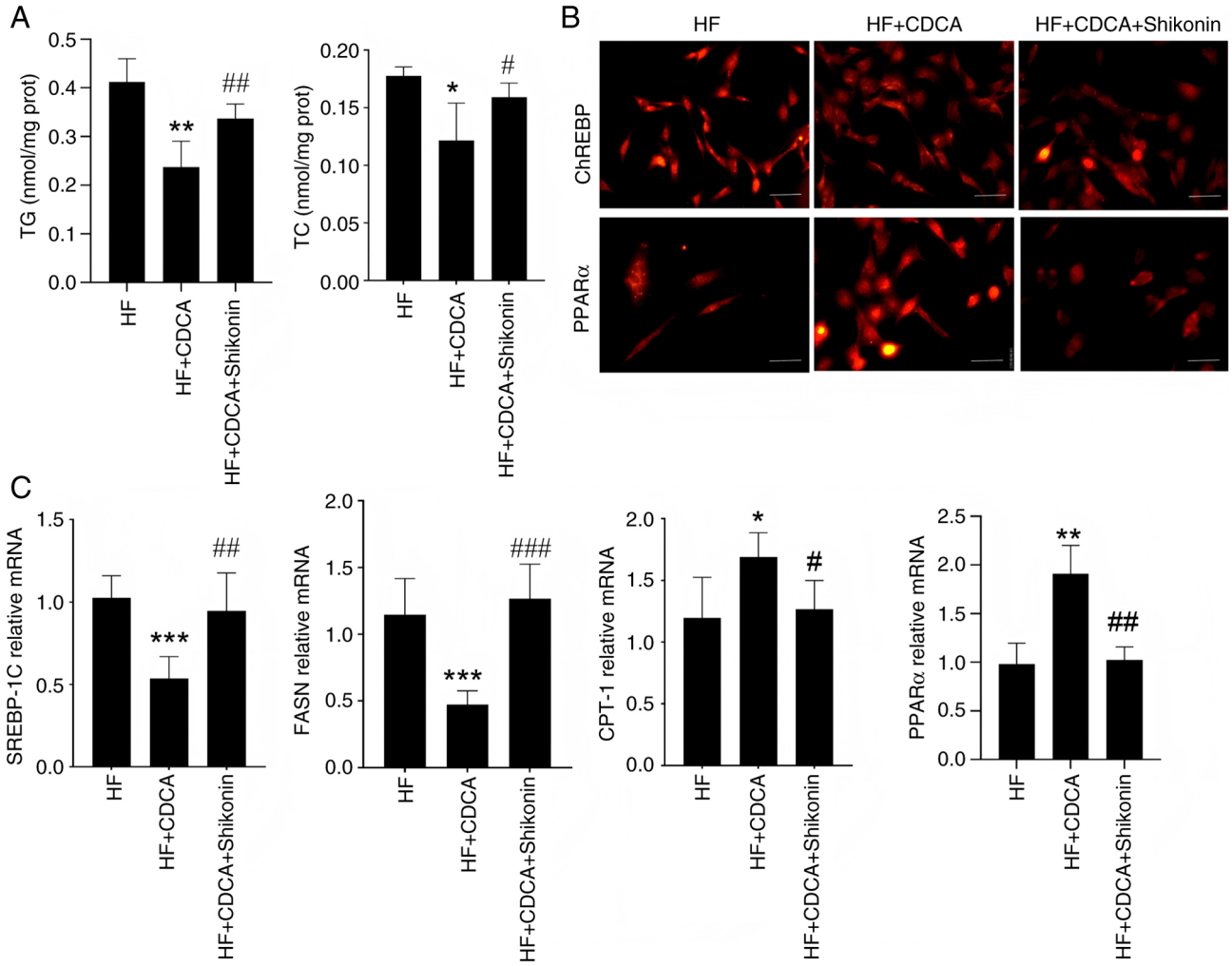

Figure 4. PK mediates the regulation of hepatic lipid metabolism by CDCA (n=4). (A) Intracellular TG and TC contents. (B) Immunofluorescence detection of ChREBP and PPARα nuclear translocation (magnification, x200; scale bar, 50 μm). (C) Reverse transcription-quantitative PCR detection of FASN, SREBP-1c, CTP1α and PPARα. *P<0.05, **P<0.01 and ***P<0.001 vs. control; $^{\#}$P<0.05, $^{\#\#}$P<0.01 and $^{\#\#\#}$P<0.001 vs. HF. Error bars represent the standard deviation. CDCA, chenodeoxycholic acid; TG, triglycerides; TC, total cholesterol; ChREBP, carbohydrate-responsive element-binding protein; SREBP-1c, sterol regulatory element-binding transcription factor 1; CTP1α, CTP synthase 1; PPARα, peroxisome proliferator-activated receptor α; HF, high fat.

in the production of pyruvate, a glycolytic product. As an important metabolic intermediate, pyruvate not only provides more substrate acetyl-CoA for fatty acid oxidation, promoting the β-oxidation decomposition of fatty acids and reducing the accumulation of hepatic fatty acids, but also, reduces *de novo* fatty acid synthesis by activating the PPARα pathway and inhibiting the expression of key lipid-synthesis genes and proteins such as FAS and SREBP-1c (14). This two-way regulatory mechanism acts simultaneously at the level of fatty acid synthesis and decomposition, effectively improving hepatic lipid metabolism and forming a novel glycolipid metabolism regulatory axis that complements the classical pathway of CDCA activation of FXR, to jointly maintain the homeostasis of hepatic lipid metabolism. PK catalyzes the formation of pyruvate from phosphoenolpyruvate and generates ATP during glycolysis, which is a key enzyme in maintaining cellular energy metabolism (15). The present study further found that PK not only serves a key role in glycolysis but also serves as a central hub in the regulation of hepatic lipid metabolism. The interaction between CDCA and PK endows PK with a novel function in lipid metabolism regulation and reveals the important role of PK in the cross-pathway of glycolipid metabolism.

Previous research has demonstrated that changes in PK activity can directly affect the activities of transcription factors such as ChREBP and PPARα, which are associated with carbohydrates (16). When PK activity is enhanced, on the one hand, it has been shown to inhibit the nuclear translocation of ChREBP, reducing the activation of the FASN promoter by ChREBP and thus inhibiting fatty acid synthesis. By contrast, it has also been shown to promote the nuclear localization of PPARα, enhance the expression of fatty acid oxidation-associated genes and promote the β-oxidation of fatty acids. This indicates that PK may act as a 'molecular switch' in the cross-pathway of glycolipid metabolism. By regulating the activities of key transcription factors, a coordinated regulation of the two major pathways of carbohydrate and lipid metabolism can be achieved. This regulatory mechanism helps to maintain the balance of carbohydrate and lipid metabolism in the liver and ensures normal physiological functions of the liver. Once the activity of PK or its interaction with CDCA is disrupted, this balance may be disturbed, leading to disorders

of hepatic lipid metabolism and further triggering metabolic diseases, such as NAFLD.

Currently, the treatment of NAFLD mainly focuses on lifestyle interventions and there is a lack of effective drug treatment methods. The discovery of the CDCA-PK axis opens a new direction for the development of novel anti-fatty liver drugs. By designing and synthesizing small-molecule compounds that can specifically enhance the interaction between CDCA and PK or mimic its effects, more effective and safer drugs for NAFLD treatment may be developed. Follow-up studies can further explore the specific regulatory roles of different PK subtypes in hepatic lipid metabolism and the synergistic mechanism of CDCA in the gut-liver axis. The gut microbiota serves an important role in bile acid and hepatic lipid metabolism. The metabolic transformation of CDCA in the intestine and its interaction with gut microbiota may affect its regulatory effect on hepatic lipid metabolism. In-depth research on these mechanisms will help to understand the regulatory network of hepatic lipid metabolism more comprehensively and provide a more solid theoretical basis for the clinical precision treatment of NAFLD.

Despite the novel findings and theoretical contributions, the present study has several limitations that should be acknowledged. First, the current research was mainly based on *in vitro* cell models and/or animal models of NAFLD; lack of clinical data from patients with NAFLD limits the translational value of the findings. Whether the CDCA-PK interaction and its regulatory role in hepatic lipid metabolism are conserved in humans, and the correlation between CDCA/PK levels and NAFLD severity in clinical populations, remain to be verified. Second, the molecular details of the direct binding between CDCA and PK-M2 were not fully elucidated. For instance, the specific binding sites on PK-M2 for CDCA, and whether this binding induces conformational changes in PK-M2 through specific amino acid residues, require further verification using techniques such as X-ray crystallography or cryo-electron microscopy. Third, the study focused on the overall regulatory effect of CDCA on PK, but did not systematically explore the potential crosstalk between the CDCA-PK axis and other bile acid-related signaling pathways (such as FXR and TGR5) in hepatic lipid metabolism. The synergistic or antagonistic effects between these pathways remain unclear. Fourth, the present study did not consider the influence of individual differences such as sex, age, and genetic background on the CDCA-PK regulatory axis. These factors may affect the response of hepatic lipid metabolism to CDCA-PK interaction, which needs to be clarified in subsequent studies. Finally, the study lacked long-term intervention experiments to evaluate the sustained effects and potential side effects of targeting the CDCA-PK axis in the treatment of NAFLD, which is essential for the development of clinical therapeutic strategies.

In conclusion, CDCA markedly improved hepatic lipid deposition, and its mechanism was shown to be closely associated with the direct binding of CDCA to PK and the enhancement of its activity. The present study not only expands the target network of bile acid-regulated metabolism, but also provides novel potential drug targets and treatment strategies for NAFLD, which has important theoretical and clinical significance.

Acknowledgements

Not applicable.

Funding

No funding was received.

Availability of data and materials

The data generated in the present study may be requested from the corresponding author.

Authors' contributions

XZhang designed and conceived the study, and was responsible for original manuscript preparation as well as review and editing. XZhang, ST and XZhou undertook data collection and analyzed the data. All authors confirm the authenticity of all the raw data. All authors read and approved the final manuscript.

Ethics approval and consent to participate

The study was approved (approval no. SW-2020R0126-F03) by the Ethics Board of Pingxiang People's Hospital (Pingxiang, China). This study was conducted in compliance with the principles of the Declaration of Helsinki.

Patient consent for publication

Not applicable.

Competing interests

The authors declare that they have no competing interests.

References

1. Riazi K, Azhari H, Charette JH, Underwood FE, King JA, Afshar EE, Swain MG, Congly SE, Kaplan GG and Shaheen AA: The prevalence and incidence of NAFLD worldwide: A systematic review and meta-analysis. Lancet Gastroenterol Hepatol 7: 851-861, 2022.
2. Yki-Järvinen H, Luukkonen PK, Hodson L and Moore JB: Dietary carbohydrates and fats in nonalcoholic fatty liver disease. Nat Rev Gastroenterol Hepatol 18: 770-786, 2021.
3. Chang TC, Chiou WC, Lai WH, Huang HC, Huang YL, Liu HK, Liang YC and Huang C: Ugonin J improves metabolic disorder and ameliorates nonalcoholic fatty liver disease by regulating the AMPK/AKT signaling pathway. Pharmacol Res 163: 105298, 2021.
4. Hüttl M, Markova I, Miklankova D, Zapletalova I, Poruba M, Haluzik M, Vaněčkova I and Malinska H: In a prediabetic model, empagliflozin improves hepatic lipid metabolism independently of obesity and before onset of hyperglycemia. Int J Mol Sci 22: 11513, 2021.
5. Murakami K, Tenge VR, Karandikar UC, Lin SC, Ramani S, Ettayebi K, Crawford SE, Zeng XL, Neill FH, Ayyar BV, *et al*: Bile acids and ceramide overcome the entry restriction for GII.3 human norovirus replication in human intestinal enteroids. Proc Natl Acad Sci USA 117: 1700-1710, 2020.
6. Xu Y, Zhu Y, Hu S, Xu Y, Stroup D, Pan X, Bawa FC, Chen S, Gopoju R, Yin L and Zhang Y: Hepatocyte nuclear factor 4α prevents the steatosis-to-NASH progression by regulating p53 and bile acid signaling (in mice). Hepatology 73: 2251-2265, 2021.

7. Du D, Liu C, Qin M, Zhang X, Xi T, Yuan S, Hao H and Xiong J: Metabolic dysregulation and emerging therapeutical targets for hepatocellular carcinoma. Acta Pharm Sin B 12: 558-580, 2022.
8. Dai P, Tang Z, Qi M, Liu D, Bajinka O and Tan Y: Dispersion and utilization of lipid droplets mediates respiratory syncytial virus-induced airway hyperresponsiveness. Pediatr Allergy Immunol 33: e13651, 2022.
9. Fan N, Zhang X, Zhao W, Zhao J, Luo D, Sun Y, Li D, Zhao C, Wang Y, Zhang H and Rong J: Covalent inhibition of pyruvate kinase m2 reprograms metabolic and inflammatory pathways in hepatic macrophages against non-alcoholic fatty liver disease. Int J Biol Sci 18: 5260-5275, 2022.
10. Liu Z, Zhang C, Lee S, Kim W, Klevstig M, Harzandi AM, Sikanic N, Arif M, Ståhlman M, Nielsen J, *et al*: Pyruvate kinase L/R is a regulator of lipid metabolism and mitochondrial function. Metab Eng 52: 263-272, 2019.
11. Bajinka O, Tang Z, Mao Y, Qiu X, Darboe A and Tan Y: Respiratory syncytial virus infection disrupts pulmonary microbiota to induce microglia phenotype shift. J Med Virol 95: e28976, 2023.
12. Deng W, Fan W, Tang T, Wan H, Zhao S, Tan Y, Oware KA, Tan J, Li J and Qu S: Farnesoid X receptor deficiency induces hepatic lipid and glucose metabolism disorder via regulation of pyruvate dehydrogenase kinase 4. Oxid Med Cell Longev 2022: 3589525, 2022.
13. Song L, Hou Y, Xu D, Dai X, Luo J, Liu Y, Huang Z, Yang M, Chen J, Hu Y, *et al*: Hepatic FXR-FGF4 is required for bile acid homeostasis via an FGFR4-LRH-1 signal node under cholestatic stress. Cell Metab 37: 104-120.e9, 2025.
14. Qiu X, Ye Q, Sun M, Wang L, Tan Y and Wu G: Saturated hydrogen improves lipid metabolism disorders and dysbacteriosis induced by a high-fat diet. Exp Biol Med (Maywood) 245: 512-521, 2020.
15. Li Z, Peng Y, Li J, Chen Z, Chen F, Tu J, Lin S and Wang H: N^6-methyladenosine regulates glycolysis of cancer cells through PDK4. Nat Commun 11: 2578, 2020.
16. Mzhel'skaya KV, Trusov NV, Guseva GN, Aksenov IV, Kravchenko LV and Tutelyan VA: Effects of quercetin on expression of genes of carbohydrate and lipid metabolism enzymes in the liver of rats receiving high-fructose ration. Bull Exp Biol Med 167: 263-266, 2019.